Biophysical Chemistry 161 (2012) 17–28

Contents lists available at SciVerse ScienceDirect

Biophysical Chemistry

journal homepage: http://www.elsevier.com/locate/biophyschem

Influence of the enzyme phosphorylation state and the substrate on PKA enzyme dynamics

Manuel Montenegro [a,1], Laura Masgrau [a,1], Àngels González-Lafont [a,b], José M. Lluch [a,b], Mireia Garcia-Viloca [a,b,*]

[a] Institut de Biotecnologia i de Biomedicina, Universitat Autònoma de Barcelona, 08193 Bellaterra, Barcelona, Spain
[b] Departament de Química, Universitat Autònoma de Barcelona, 08193 Bellaterra, Barcelona, Spain

HIGHLIGHTS

- The Thr197 phosphorylation site seems to be necessary for the enzyme function.
- The different phosphorylation states influence the flexibility of the structure.
- Asp166 is crucial for the correct placement of the P-site of the substrate.
- Asp 166 has an active role in limiting the accessibility to the active center.

GRAPHICAL ABSTRACT

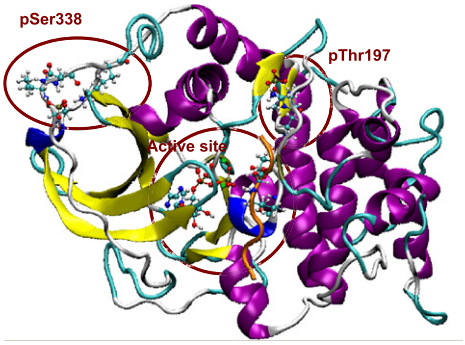

ARTICLE INFO

Article history:
Received 14 April 2011
Received in revised form 4 November 2011
Accepted 6 November 2011
Available online 17 November 2011

Keywords:
Enzyme phosphorylation state
Enzyme dynamics
Asp166Ala mutation
Pre-reactive contact

ABSTRACT

cAMP-dependent protein kinase (PKA) is one of the simplest and best understood members of the protein kinase family. In a previous study, we have theoretically studied the complex between PKA and the heptapeptide substrate Kemptide by classical molecular dynamics. On the basis of the results obtained for Kemptide, the aim of the present work is to explore how the different conditions, such as phosphorylation state, substrate, and mutations of key residues affect the enzyme dynamics. We have built different models of the complex; particularly we have focused our attention on two crystallographic structures which main difference consists in their phosphorylation state. The first one has the residue Thr197 modified into a phospho-threonine (pThr197); the second one, in addition to the same Thr197, has also the residue Ser338 modified into a phospho-serine (pSer338). In addition, we have analyzed the effect of the choice of the substrate by building a model of the PKA-SP20 Michaelis complex. Finally, we have theoretically studied the effect of the mutation of the highly conserved residue Asp166 that, experimentally, leads to a decrease of the reaction rate. The results of this study give insight into the dynamical states of the enzyme and their relationship with different elements of the model, which correspond to different natural or human guided situations of the active biological system.

1. Introduction

In 1955 was first elucidated that protein phosphorylation, catalyzed by protein kinases, is likely the most important mechanism for regulation in mammalian cells [1]. Protein kinases are highly dynamic proteins that can toggle between different conformational states that allow them to serve as molecular switches. Most protein

* Corresponding author at: Unitat de Química Física, Departament de Química, Edifici Cn, Universitat Autònoma de Barcelona, Spain. Fax: +34 935812920.
E-mail address: mireia@klingon.uab.cat (M. Garcia-Viloca).
[1] Both authors contributed equally to the work.

0301-4622/$ – see front matter © 2011 Elsevier B.V. All rights reserved.
doi:10.1016/j.bpc.2011.11.001

kinases have phosphorylation sites that are an integral determinant for both structure and function. They can serve as docking sites for other proteins or as organizing points that lock the kinase itself into a conformation that is optimal either for catalysis or for inhibition. Often, correct assembly of the active kinase depends on the critical addition of a phosphate [2].

Within the large and very diverse family of protein kinases, cAMP-dependent protein kinase (PKA), first characterized in 1968, [3] is one of the best understood members. As a consequence, it is often used as a prototype for the entire family. It is an ideal system to study because of the fact that it is comprised of two types of subunits that are dissociated upon activation by cAMP. Thus, the inactive holoenzyme consists of two regulatory (R) and two catalytic subunits. Once the catalytic subunits are released, they are active proteins, which can be overexpressed in *Escherichia coli* as fully active proteins [2]. PKA has another class of physiological inhibitor apart of the R subunits, the heat-stable protein kinase inhibitor (PKI), which also binds with high affinity to the free catalytic subunit [4].

The catalytic subunit of PKA is comprised of a bilobal core that is shared by all members of the protein kinase superfamily. It has a conserved catalytic core, shared by all Ser/Thr- and Tyr-specific protein kinases, consisting up of about 220 residues. Different conserved loops (see Fig. 1) are found in the large lobe of the catalytic core, which have received different names:

The *catalytic loop (residues 165–171)* contains highly conserved residues with Asp166 positioned near the hydroxyl proton of the peptide substrate, and Lys168 interacting with the γ-phosphate of ATP. Mutation to Ala causes at least a 300-fold reduction of the v_{max} without greatly affecting the K_ms for either ATP or the substrate peptide [5].

The *activation loop (residues 195–197)* contains the highly conserved Thr197 residue, which is phosphorylated in all the structures that have been resolved to date. It is the phosphorylation of the activation loop by another protein kinase that is essential for activation [2,6,7].

Magnesium positioning loop (residues 184–190) also contributes to catalysis by Asp184 binding to the magnesium ion that bridges the β- and γ-phosphates of ATP. In addition, the highly conserved Phe187 helps to exclude water from the site of phosphoryl transfer.

Peptide positioning loop (residues 198–280): The segment of residues that touches and contributes to the positioning of most parts of the consensus site substrate peptide (P − 3 through P + 1, that is Arg-Arg-Ala-Ser-Leu, where Ser occupies the P-site).

In PKA there is a second phosphorylation site, residue Ser338, in the C-terminal tail, which consists of 50 residues that wrap around the surface of the conserved core. Ser338 is not always phosphorylated in the structures resolved to date. However, the mature enzyme isolated from mammalian cells is phosphorylated on Thr197 and Ser338; both of these phosphates are very stable. Replacement of Ser338 with Ala destabilizes the enzyme [2].

On the basis of the conserved catalytic core, it is believed that protein kinases share a common mechanism, although it has not been yet clarified. The actual two possibilities are shown in Fig. 2 and have been explored by several theoretical and experimental grups [2,7]. In Fig. 2a, the so called associative mechanism is represented, whereas the dissociative mechanism is shown in Fig. 2b. The names associated to them are related to a quantitative model proposed by Mildvan, based on the distance between the nucleophilic Ser17 oxygen and the γ-phosphorous of ATP [8]. More importantly, from a qualitative point of view, Fig. 2(A) shows two mechanisms which

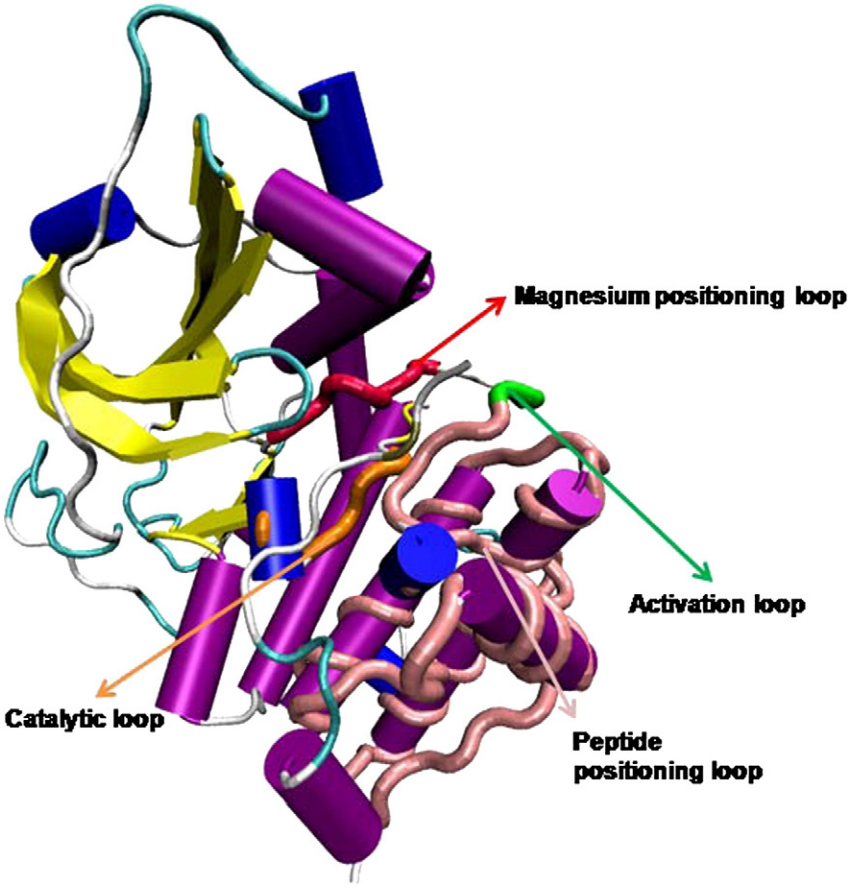

Fig. 1. Protein kinase motifs: catalytic loop (in orange), activation loop (in green), magnesium positioning loop (in red), and peptide positioning loop (in pink).

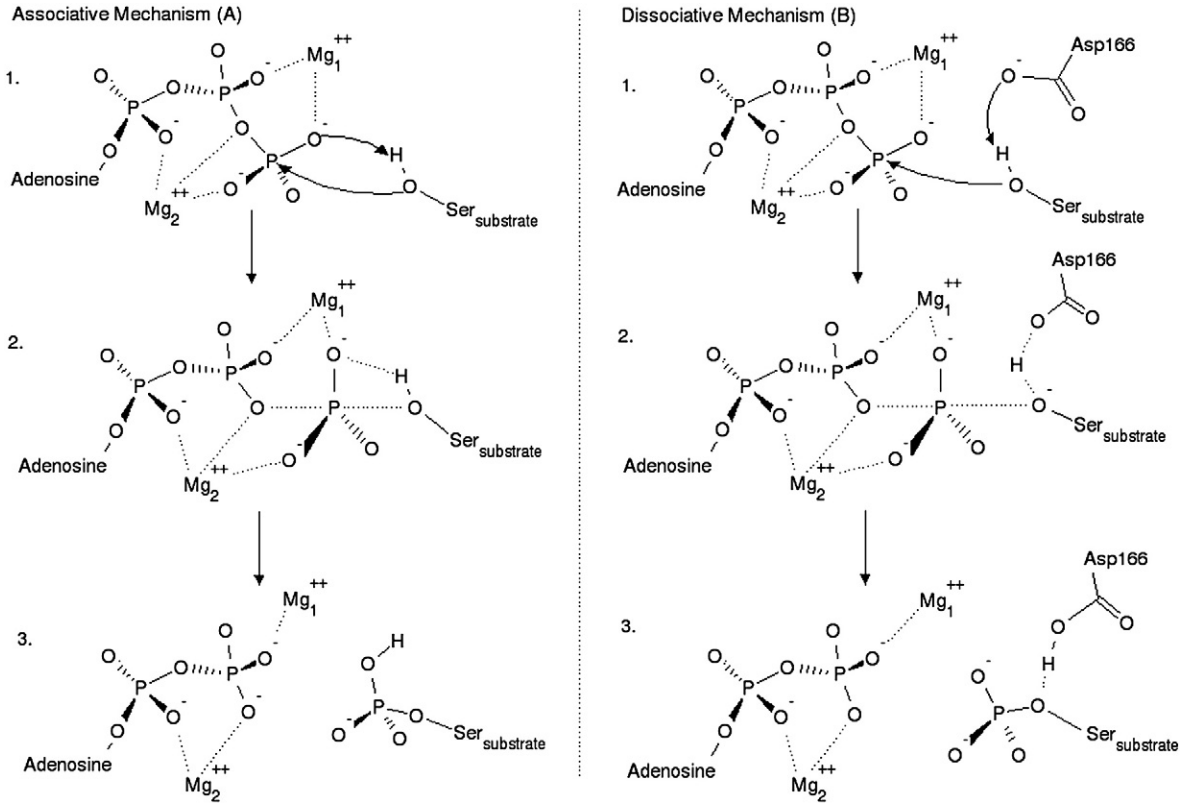

Fig. 2. Reaction scheme for the phosphoryl transfer step: Scheme A is the associative mechanism which consists in the phosphoryl- and proton-transfers between the substrate and the ATP molecule. Scheme B represents the dissociative reaction pathway; the proton of Ser17 passes to an oxygen of Asp166 during the nucleophilic displacement.

consist in the concerted phosphoryl- and proton-transfers between the substrate and the ATP molecule, whereas Fig. 2(B) represents the asynchronous transfer of Ser17 proton to Asp166 during the nucleophilic displacement.

As other kinases, PKA has been shown to be an enzyme that recognizes a restricted region of the local sequence around the phosphorylation site. In the case of PKA that is Arg-Arg-X-P-Z, where X is a small residue, P is the residue to be phosphorylated and Z a large hydrophobic one. Substrates of different size have been used in recent experimental [9,10] and theoretical studies [11,12]. As shown in Table 1, the experimental results found in the literature indicate that the kinetic properties of the enzyme depend on the nature of the substrate, but this issue has not been analyzed in the previous theoretical studies.

In a previous study, we have theoretically studied the complex between PKA and the heptapeptide substrate Kemptide by classical molecular dynamics [13]. In that work, we chose Kemptide as target substrate because detailed thermodynamic and kinetic experimental analyses have been performed on the phosphorylation of this efficient peptide [14–16], but it has not been used in previous theoretical studies. We have demonstrated its dynamical stability and its most important prereactive contacts in the active site of PKA, which determine substrate specificity [13]. On the basis of the results obtained for Kemptide, the aim of the present work is to explore how the different conditions, such as phosphorylation state, substrate, and mutations of key residues affect the enzyme dynamics. The results of this study give insight into the dynamical states of the enzyme and their relationship with different elements of the model, which correspond to different natural or human guided situations of the active biological system.

Table 1
Different peptide substrates of PKA and their catalytic constants reported in the literature.

Substrate	Sequence	k_{cat} (s^{-1})
Kemptide	LRRASLG	22 ± 2[a]/500[b]
SP20	TTYADFIASGRTGRRASIHD	1.8 ± 10[a]
Peptide model	GRTGRRNSI	154[b]

[a] Ref. [9].
[b] Ref. [11].

We have built different models of the complex; particularly we have focused our attention on two crystallographic structures which main difference consists in their phosphorylation state: amongst all the available structures, we have chosen those with PDB-ID-codes 1CDK [17] and 1ATP [18]. The first one has the residue Thr197 modified into a phospho-threonine (pThr197); the second one, in addition to the same Thr197, has also the residue Ser338 modified into a phospho-serine (pSer338).

In addition, we have analyzed the effect of the choice of the substrate by building a model of the PKA-SP20 Michaelis complex, starting from the 1ATP crystal structure, as previously done by Cheng et al. [7,19]. The results have been compared to the PKA-Kemptide model.

Finally, in order to provide a deeper insight of the functioning of the kinases, we have built two supplementary models based on the 1CDK crystal structure and the Kemptide substrate, and analyzed their behavior along molecular dynamics simulations. In one model, we have modeled a deactivated form of the enzyme, in which both phosphorylation site residues of PKA are not phosphorylated. In the other, we have modified Asp166 of 1CDK to an alanine, thus building the D166A model.

At the end, this paper wants to be a complement to the experimental studies devoted to PKA. As noted by Taylor and collaborators [2], X-ray crystallography provides only snapshots of specific conformations, but it is not possible to form crystals of all functional conformations and configurations of the protein, and in this sense,

molecular dynamics studies like the one presented in this paper provide dynamical information that is difficult to obtain from experimental works.

2. Computational details

2.1. Model of the enzyme–cofactor–substrate Michaelis complex

To build the models of the biological system, the starting coordinates of the catalytic subunit were taken either from the crystallographic structure with PDB-ID-code 1CDK [17] or from the one with the code 1ATP [18]. Both correspond to the closed active conformation of the enzyme. As they are from different organisms the sequences are not the same but the only significant difference consists in the number of phosphorylated amino acid residues, one in the case of 1CDK and two in that of 1ATP.

In the case of 1CDK, the crystallographic structure contains the enzyme catalytic subunit, an ATP analog (AMP-PNP), two Mn^{++} ions, a 20-residue peptide inhibitor (PKI(5–24)), and 149 water molecules. Our system was built changing the Mn^{++} ions to the biologically active Mg^{++} ions and the AMP-PNP molecule to ATP. In order to maintain the active configuration of PKA we kept at position 197 the phosphorylated threonine. The Kemptide was positioned in the active center of PKA by manually modeling it from the PKI(5–24) inhibitor, which is bound to the enzyme in the X-ray structure. With respect to the inhibitor crystallographic structure, we have deleted all the residues from Thr1 to Thr12 and the last one, Asp20. Then, we have modified the remaining residues to obtain the Kemptide substrate: we changed Gly13 to Leu13, Asn16 to Ala16, Ala17 to Ser17, Ile18 to Leu18, and His19 to Gly19. This model has been used in a previous study where it has been equilibrated and its stability has been demonstrated by a 6 ns molecular dynamics simulation. Further details about the model can be found in a recent paper [13].

In the case of 1ATP we proceeded practically the same way, with just some minor differences. First of all, we have substituted the two Mn^{++} ions with Mg^{++} ions, then we modeled two substrates in the catalytic center generating two different models: the first one with the Kemptide as target substrate, for which we have proceeded exactly as in the preceding model; the second one with the SP20 peptide as substrate, for which we simply modified the original asparagine in the 16th position of the PKI(5–24) inhibitor into an alanine and the original alanine in the 17th position into a serine. We will call the first model 1ATP-Kemp and the second one 1ATP-SP20. The original crystallographic structure already contains an ATP molecule bound, thus no modifications were performed with respect to this aspect.

As explained in our previous work on the 1CDK model [13], the HBUILD facility has been used to correctly position the hydrogen atoms, but in the case of 1ATP-Kemp and 1ATP-SP20 models, for the protonation state of the histidine residues we followed the work of Cheng et al. [19], in which the same crystallographic structure is used to build the model. Thus His62, His68, and His260 were protonated at nitrogen δ; His131, His142, His158, and His294 were protonated at nitrogen ε; and the residue His87 was doubly protonated. In 1ATP-SP20 another histidine is present at the 19th position of the substrate; its protonation state has been calculated with the program PROPKA [20] as no indication are given in the work of Cheng et al. [19], and thus in our model it has been protonated at the nitrogen δ.

In order to neutralize the positive charge of the obtained structures we placed four Cl^- anions in the proximity of positively charged residues and as far as possible from the active center of PKA in the 1ATP-Kemp model, and similarly we added three Cl^- anions in the 1ATP-SP20 model.

The origin of the system was then adjusted to the geometrical center of the $C_{\gamma\text{-Asp166-PKA}}$, $P_{\gamma\text{-ATP}}$, and $O_{\gamma\text{-Ser17-kemp}}$ group of atoms (atoms in the Michaelis complex active core). The energy of the atoms within a sphere of 20 Å around this point was minimized by 50 steps. Then, a box of TIP3P water molecules centered at the origin was added. The initial dimensions of the water box for 1CDK were 82 Å × 68 Å × 65 Å and for 1ATP were 91 Å × 73 Å × 77 Å to ensure a distance of at least 10 Å between the enzyme and the box edges. Water molecules of the box located within 2.5 Å of any non-hydrogen atom of the solute (PKA, ATP, Kemptide, Mg^{++} ions), crystallographic waters, or anions were removed. The total number of atoms is 54352 and 51600 for the 1ATP-Kemp and 1ATP-SP20 models, respectively.

2.2. Equilibration

The Michaelis complex represented by the model system was first studied by carrying out a classical molecular dynamics simulation with the all-atom CHARMM22 force field [21]. For the phosphorylated Thr197 and Ser338 we have used the standard parameters included in the CHARMM version 31 (c31) parameter files [22], which were optimized against experimental data and ab initio calculations [23].

We first removed the close contacts and the repulsive orientations of the system by carrying out energy minimizations in two steps. First, 200 steps of energy minimization of the solvent molecules (water and Cl^-) were performed, followed by 100 steps of optimization of all the atoms coordinates. The energy minimization method was the adopted basis set Newton–Raphson (ABNR) implemented in CHARMM version c31 [22].

Finally, starting from the resulting structure, we carried out molecular dynamics (MD) simulations with periodic boundary conditions (PBC) in the isothermal–isobaric ensemble at 296 K and 1 atm. These simulations were performed with the CRYSTAL routine of CHARMM c31: the program generates 26 images identical to the primary cell (complex plus water box) all around it; only the images within a cutoff distance (20 Å) were built in order to decrease the number of nonbonded interactions. In this work a spherical cutoff of 13 Å together with a switching function to fade the interaction energy to zero was used for the non-bonded interactions. The switching function acts between 11.5 Å and 12.5 Å. On the base of neutral-groups separations, the nonbonded pair list was updated every 25 steps while the image list was refreshed every 100 steps. To compute the contributions of long range electrostatic interactions, we used the Particle Mesh Ewald method with a grid spacing of ~1 Å and a fourth-order B-spline interpolation to calculate the potential and forces between grid points.

The propagation of the equations of motion was accomplished with the leapfrog integration scheme, a 2 fs time step, and the extended system constant pressure and temperature algorithm implemented in CHARMM. All bond lengths were constrained by SHAKE and the dielectric constant was set to 1.

The initial temperature was gradually raised from 0 K to 296 K with a 68 ps or 100 ps restrained MD simulations (depending on the model). Harmonic potentials centered on the crystallographic positions were used for the backbone atoms of the protein and the substrate, for the heavy atoms of the ATP molecule, and for the two Mg^{++} ions. Then the restraints were gradually removed during 100 ps of simulation at 296 K, which was followed by a MD simulation of the unrestrained system for 100 ps more. The resulting structure was taken as the starting point for all the data presented in the present work. The total length of the reported free MD simulations was approximately 11 ns and 6 ns for the 1ATP-Kemp and the 1ATP-SP20 models, respectively. Structural data was saved every 100 steps of the simulation for later analysis.

In addition, two tests have been carried out with the two slightly modified forms of the PKA enzyme. Both modifications have been performed starting from the already equilibrated 1CDK model, in order to observe the response of the system. The first one is a deactivated form, which is the PKA enzyme without any phosphorylated residue, neither the Thr197 nor the Ser338. With the second one,

we have studied another modified model of the holoenzyme. In this case the Asp166 residue has been mutated by an alanine residue, hence the name D166A for this model. We have carried out 6 ns and 11 ns of MD simulations for the deactivated and mutated forms of the enzyme, respectively.

3. Results and discussion

3.1. 1ATP-Kemp

In a similar way as in the previous paper on the results obtained for the 1CDK model [13], we now present the same structural analysis on a different model. We remind, at this point, that the main and most interesting difference between the 1ATP-Kemp model and the previous one [13], is the phosphorylation of the Ser338 (pSer338), modification that is absent in the 1CDK model. Ser338 is a residue located in the C-terminal tail of the enzyme which is different in all protein kinases and is thought to be relevant for the substrate selection [2]. Thus, it is not present near the active center of the system and has no direct interactions (through H-bonds) with the residues surrounding it. Nevertheless, as we will discuss later on, it seems to have an important effect on the enzyme dynamics and catalytic mechanism.

In Table S1 of the Supporting Information the Mg–ligands distances obtained after the 11 ns MD simulation, along with three reference distances, are reported. It can be seen that the values are in very good agreement with the experimental data, taking into account that in the X-ray structures there are two Mn^{++} ions instead of two Mg^{++} ions. The obtained values for 1ATP-Kemp are almost the same as the ones presented in Table S1 of Ref. [13], with only small differences present, probably due to the natural movement of the structures along the equilibration. The small fluctuations of the distances reported indicate the high stability of the model.

From the analysis of the root mean square deviations (RMSDs) of the 1ATP-Kemp model, we have found a different pattern from the one of the 1CDK [13]. In both cases the reference structure used corresponds to the protein and ligand backbone coordinates in the crystallographic structure. In the 1CDK case, the RMSD deviation analysis of the Kemptide backbone showed a sudden jump at about 2 ns of the simulation that was attributed to the high mobility of the N-terminus part of the substrate [13]. Instead, for the 1ATP-Kemp model, the RMSDs of the backbone of PKA and of Kemptide, as showed in Fig. 3a and b, respectively, do not present sudden jumps along the simulation. That is, just a few pikes of higher amplitude than the average trend can be noticed in the RMSD of PKA, while only minor oscilations can be seen in the Kemptide's RMSD. This leads us to the hypothesis that the phosphorylation of Ser338 (present in the 1ATP-Kemp model only) results in a greater rigidity of the enzymatic system.

Nevertheless, even if no puzzling movements of Kemptide can be highlighted looking at Fig. 3b, we checked the stability of the substrate as done before, dividing the heptapeptide in three portions and calculating the RMSDs separately. Thus we have considered Leu13 and Arg14 as the N-terminal part, Leu18 and Gly19 as the C-terminal part, and Arg15, Ala16, and Ser17 as the central portion. As expected, the three RMSDs, presented in Fig. S1, do not show important movements of the segments: it can be seen how, in the 1ATP-Kemp model, even the C-terminal portion (blue line in Fig. S1), which is the one with less anchorage point, is very stable along the whole simulation.

As a further confirmation of the stability of Kemptide, we can observe the conformation of the side chain of the P-site serine. In Fig. S2 of the Supporting Information the distribution of the Ser17 side chain torsion along the molecular dynamics is represented. From this Figure it can be seen that the predominant rotameric state is G^+, as found in our 1CDK model and in agreement with the results reported by Cheng et al. [7] for a model built from the 1ATP crystallographic structure with the SP20 substrate.

At this point, it is worthy to remark that the interactions found between Kemptide and PKA along the simulation of the 1ATP-Kemp model are very similar to the ones reported for our 1CDK model and thus, we will not comment them further.

Next, we will focus our attention on the most significant distances in the active center, i.e. the distances involving the hydroxylic oxygen of

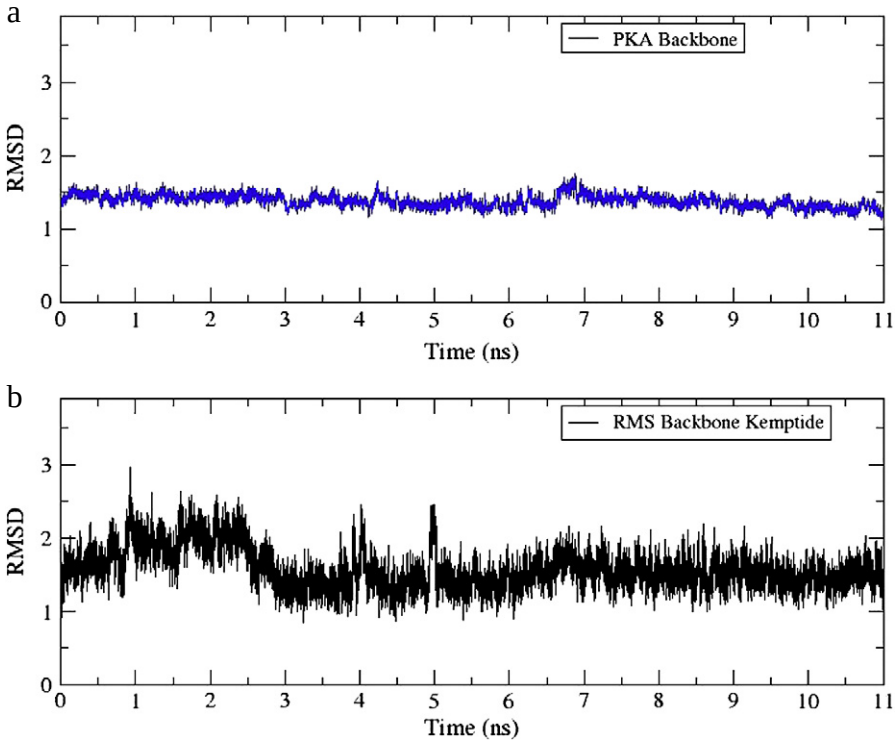

Fig. 3. RMSDs of a. PKA backbone and b. Kemptide backbone, in the 1-ATP Kemp model.

Ser17. In Fig. 4 the trends of all the interaction distances of $O_{\gamma\text{-Ser17-Kemp}}$ are depicted. In the upper part, the distances between Ser17 and ATP can be observed. It can be seen that, after an initial uneventful period that lasts for approximately 2.5 ns, the system undergoes a rearrangement that leads to an overall increase in the distances between the substrate and the cofactor. Also in this model the average distance between $O_{\gamma\text{-Ser17-Kemp}}$ and $P_{\gamma\text{-ATP}}$ turns out to be 4.02 ± 0.47 Å, approximately in the middle between the two limiting values proposed by Mildvan [8] (3.3 Å for the mechanism to be associative and greater than 4.9 Å for the mechanism to be dissociative). There is an initial jump from one configuration to the other (that is, from a lower value to an upper one and vice versa) but beyond the first 2.5 ns the reported distance fluctuates around the average value.

Some other information, perhaps more interesting, can be inferred from the lower part of Fig. 4, where the distances between the O_γ of Ser17 and several atoms of the enzyme are presented. Foremost, looking at the distance between $O_{\gamma\text{-Ser17-Kemp}}$ and $N_{\zeta\text{-Lys168-PKA}}$ we can observe that its value is the same as in the 1CDK model (Fig. 7 Ref. [13]), but the oscillations around the middle point are smaller than in the case of 1CDK, that is, the oxygen is bound more tightly to the positive side chain of lysine.

In regards to the interaction between $O_{\gamma\text{-Ser17-Kemp}}$ and $O_{\gamma 1\text{-Thr201-PKA}}$, Fig. 4 shows that from an initial weak interaction, the simulation takes the residues to a distance at which the interactions are virtually non-existent, with spikes over 7 Å. This is a different result than the one found in the 1CDK model (Fig. 7 Ref. [13]), where this interaction is conserved along the simulation.

Finally, we can observe the trends of the distances between $O_{\gamma\text{-Ser17-kemp}}$ and the two carboxylic oxygen atoms of Asp166, that with respect to the 1CDK model are smaller for both carboxylic oxygens. In this case, both atoms remain at a distance of about 3 Å from Ser17, switching places with one another as they go on rotating around the carboxylic carbon atom.

In conclusion, the simulation of 1ATP-Kemp leads only to one state, with small fluctuations around the average distance values, which suggests, for all the reasons previously commented (the average distance between the γ-phosphoryl group of ATP and the hydroxylic group of $Ser17_{Kemp}$, the presence of quite a strong interaction, all through the simulation, between the latter group and one of the carboxylic oxygen atoms of $Asp166_{PKA}$, and finally, the small degree of flexibility of the model) that the dissociative mechanism might be more probable.

3.2. 1ATP-SP20

As a comparative test, we have built a third model of the system, this one based on the model used by Cheng et al. [7,19]. The purpose was to find out possible differences in the behavior of our models and to further understand the mechanisms and the key factors underlying the chemical structure. In this model, called 1ATP-SP20, we have used the X-ray structure with PDB-ID-code 1ATP as the base of our system, and modeled the substrate peptide SP20 upon the inhibitor PKI(5–24) by simply changing the Asn16 into Ala16 and Ala17 into Ser17. Thus, the main differences between the 1CDK model [13] and this one consist in the phosphorylation state of Ser338 and in the presence of a longer substrate bound to the catalytic core of the enzyme.

As in the previous models described here and in Ref. [13], the stability of the model has been assessed by the interaction distances between the Mg^{++} ions and their ligands (Table S2) together with the RMSDs of the enzyme and the substrate (Fig. S3). It is worthy to remark that probably because of the high degree of similarity between our model and the original X-ray structure (we have basically substituted the two metal ions in the catalytic center, and two residues of the inhibitor), the reported RMSDs show that the system barely moves along the simulation and that both the enzyme and the substrate seem to be quite stable in their own configuration since the very beginning. Only the substrate undergoes a little movement at about 1 ns, but no excessively high values or sudden jumps can be noticed along the simulation.

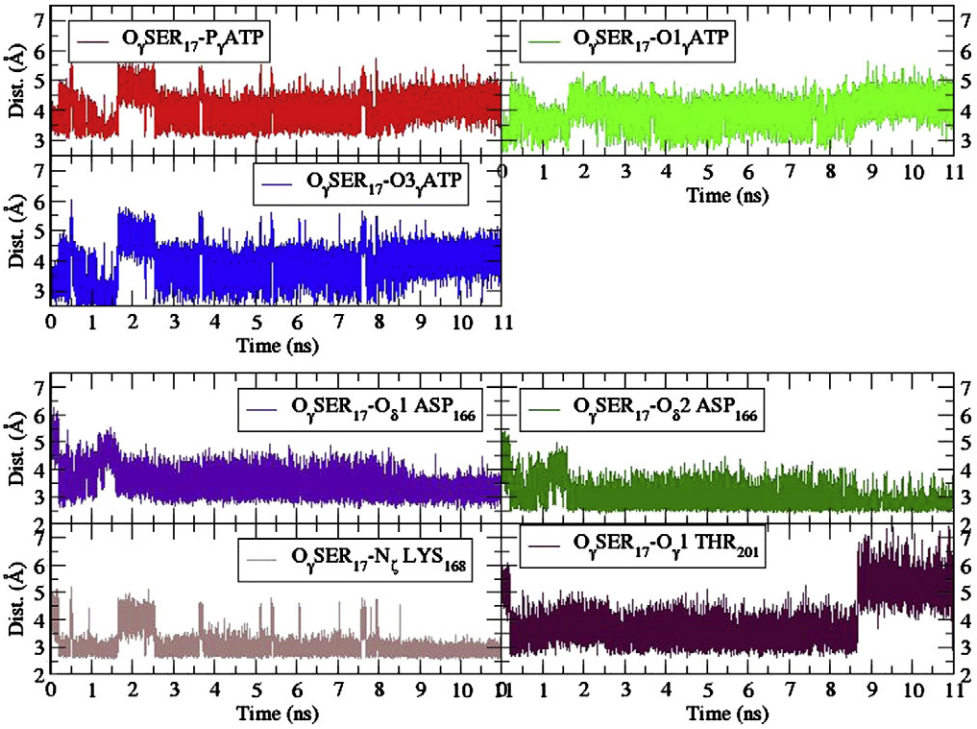

Fig. 4. Evolution of the interaction distances involving Ser17 through the MD simulation in the 1ATP-Kemp model. In the upper part the interaction distances of Ser17 with ATP are represented. In the lower part the interactions of Ser17 with some residues of PKA are depicted.

To be coherent with what was presented in the previous subsections, we further analyzed the RMSD of the SP20, and, focusing only on the seven-residue portion of the substrate directly comparable with Kemptide, we divided it into three segments and calculated their RMSDs separately. In Fig. S4 the corresponding RMSDs of the substrate portions are depicted. Surprisingly enough, we have found that from Gly17 to Ser21 (first and central part of the peptide) the residues are almost frozen in their positions with only small fluctuations around the average configurations, but the last two residues analyzed, corresponding to the C-terminus of Kemptide, seem to be fairly unbound and free to move in comparison to the other residues and, more importantly, to the 1ATP-Kemp model (Fig. S1).

Another quite unexpected result is shown in Fig. S5 where the torsion distribution of the P-site serine side chain is presented. Contrarily to the results that we have obtained in the other two cases (Fig. 6 Ref. [13] and Fig. S2), and to what Cheng et al. [7] have presented in their work, in our MD simulation of the 1ATP-SP20 model the side chain of the serine seems to prefer a torsion between 60° and 70°, with a sharper distribution with respect to the 1CDK model. This result is a consequence of the different orientation of the serine O atom, which tends to remain in a different position than in the previous two models, just on the opposite side with respect to Asp166.

The direct consequence of the stability and steadiness of this model can be observed looking at the interaction distances of the P-site serine. In Fig. 5 the trends of the main interactions involving the alcoholic oxygen of the serine are depicted. No other distances will be presented in this subsection because, as already mentioned in the previous subsection, the model does not show any noticeable difference in the distances between the internal residues, thus no significant information can be added to the analysis by further commenting on them.

In the lower part of Fig. 5 the distances between the P-site serine and some enzyme residues of interest can be observed. At a first glance, the Figure shows the stability of the selected interactions. The evolution of the four distances depicted tends to a highly steady average distance with fluctuation not big enough to consider that there might be a possible change in the conformation. It is interesting to underline that all these interaction distances are larger than the counterparts presented for the other models; even the distance with Lys168 side chain is too long to allow the formation of an H-bond. In the upper part of the Figure we can observe the trends on the distances between the O_γ atom of the serine and the atoms of the γ-phosphoryl group of ATP, and, once again, the almost complete absence of movement is deduced from the Figure. This time, the distances are smaller than those of the other models and, particularly, the $P_{\gamma\text{-ATP}}$-$O_{\gamma\text{-Ser21-SP20}}$ distance has an average value of 3.48 Å, quite similar to the lower limit distance given by Mildvan for the associative mechanism prereactive state [8].

In conclusion, the results presented in this subsection, which includes the stability of the model, the distance between the P-site serine and the γ-phosphoryl group, the distance between the serine and Asp166, the torsion of the side chain of Ser21, and the overall steadiness of the catalytic center, lead us to the conclusion that the 1ATP-SP20 model presents all the favorable conditions for the associative mechanism, in contrast to the result obtained in previous theoretical works [7,19]. The disagreement between them might be explained through the hypothesis that the system could be too rigid to allow conformational changes.

The cause of the rigidness of this last model is most likely due to the presence of extra residues in the SP20 peptide with respect to Kemptide. These extra residues are not free to move, but instead make this substrate and the PKI inhibitor tightly bound to the enzyme.

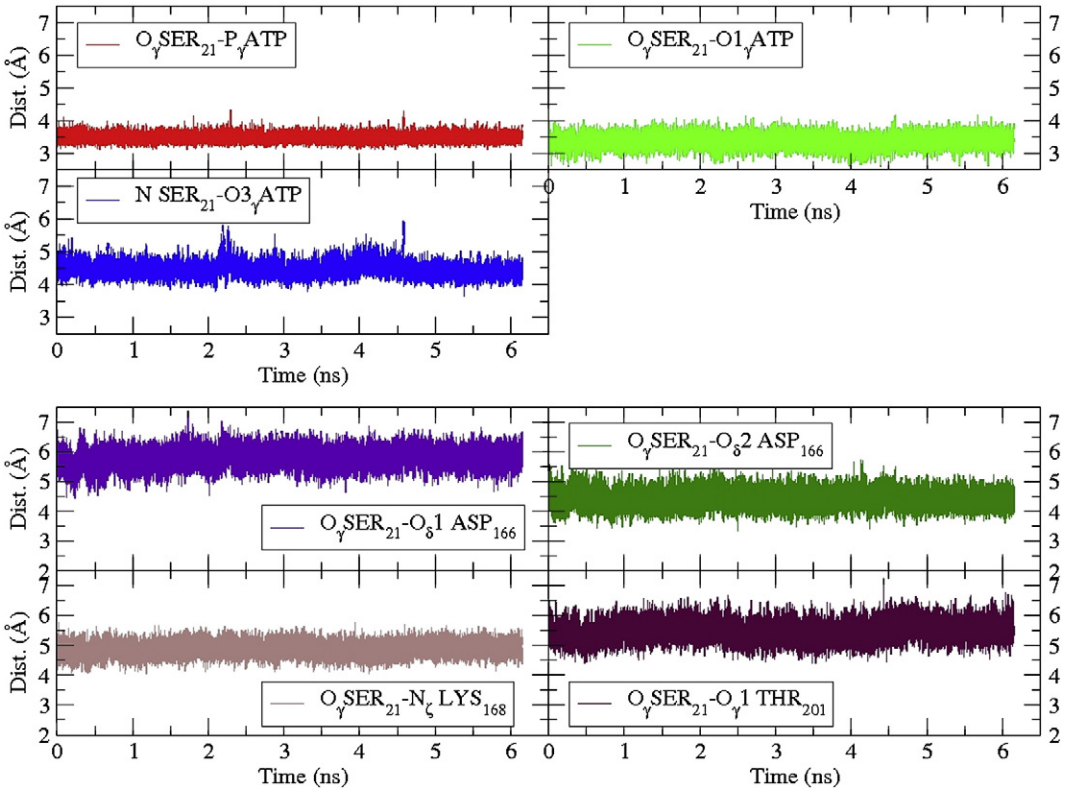

Fig. 5. Evolution of the interaction distances involving Ser21 throughout the MD simulation in the 1ATP-SP20 model. In the upper part the interaction distances of Ser21 with ATP are represented. The interactions of Ser21 with some residues of PKA are depicted in the lower part of the Figure.

3.3. 1CDK deactivated form

In this and the next subsection we are going to briefly discuss the results of two simulations carried out with the two slightly modified forms of the PKA. Both modifications have been performed starting from the already equilibrated 1CDK model, in order to observe the response of the system. The first one is a deactivated form, which is the PKA enzyme without any phosphorylated residue, neither the Thr197 nor the Ser338. In this model these two residues cannot form the H-bonds that they establish in the phosphorylated state through the phosphoryl group. In Fig. 6 the structure of the doubly phosphorylated form of PKA is depicted. The picture is meant to show the relative positions of the two phosphorylated residues and that of the active center, highlighted with red circles. The distances between $O_{\gamma\text{-Ser17-kemp}}$ and the phosphorous atom of $pThr197_{PKA}$ and $pSer338_{PKA}$ are 12.47 Å and 30.47 Å, respectively.

The case of Thr197 is especially interesting, since, when phosphorylated, it forms two H-bonds with the guanidinium protons of Arg165. This last residue is directly connected through the backbone atoms to Asp166 and thus, the Thr197–Arg165 interaction seems to have a key role in the orientation of the catalytic Asp166 residue in the active center.

In Fig. 7 the RMSD of the deactivated PKA backbone (upper section) is represented respect to the protein and ligand backbone coordinates in the crystallographic structure, together with the RMSDs of the two regions where Thr197 and Arg165, Asp166, and Lys168 are situated, respectively named coil 197 and coil 165 (lower section). The whole backbone does not show any evident movement, but a slow and continuous rise in the RMSD value can be noticed: at the beginning the average value is lower than 1 Å, but at the very end it is increased by about 50% of the initial value, and the fluctuations around the average are rather small all through the simulation, which means that the movement of the protein is not a simple respiration, but rather a slow conformational change from the active form to the inactive one.

The observation of the RMSDs of coils 167 and 165 gives us some other interesting information about what is happening in the active center. Foremost, the movement of the coil 197 (black line), where Thr197 is located is quite evident. At the very beginning the RMSD value jumps from about 0.5 Å to about 1.5 Å and, after the first nanosecond of the simulation starts increasing again reaching the value of about 2.5 Å with evident fluctuations around the average. This leads to the conclusion that the H-bond interactions between pThr197 and Arg165 are needed to maintain the configuration, and their absence leaves the coil free to move in a wide space. As a consequence, the distance between the alcoholic oxygen of Thr197 and the nearest nitrogen of Arg165 is 3.76 Å at the beginning, 7.24 Å at 3 ns, and 6.72 Å at 6 ns. In Fig. 8 schematic representations of the main interaction distances of the deactivated model are depicted.

On the other hand, the RMSD of coil 165 remains at the value of about 0.5 along the whole simulation. Nevertheless, a variation in the fluctuations can be noticed: they become slightly but perceptibly smaller going from the beginning to the end, indicating that the residues in this region (Arg165, Asp166, and Lys168) reach a more stable configuration with respect to the initial destabilized conformation, increasing the strength of their interactions. Indeed, the distance between $C_{\gamma\text{-Asp166-PKA}}$ and $N_{\zeta\text{-Lys168-PKA}}$ changes from the initial value of 3.25 Å to 3.20 Å at 3 ns and then remains constant until the end of the simulation. As a consequence, while one of the two Asp166 carboxylic oxygen atoms remains at the distance of 2.71 Å from the Lys168 nitrogen throughout the whole simulation, the other one passes from the initial distance of 3.02 Å to the final distance of 2.84 Å.

Finally, Fig. 9 shows the RMSD of the Kemptide backbone, along with its last 3-residues backbone RMSD. The Fig. 9a shows an increase of the average value almost continuously along the MD simulation, from an initial value of 0.7 to a final one greater than 2.5, without coming to a stable configuration. Analyzing the trend of the second RMSD depicted in the lower Figure, it shows that the 3-residue C-terminus section of Kemptide (blue line in Fig. 9), where the P-site serine is located, contributes to the increasing of the overall RMSD: the value goes on increasing along the 6 ns, which is an indication of the deactivation, and apparently, it would follow the same trend even after.

Focusing on the interaction distances, we have observed a large change in the position of the P-site serine, and thus in the

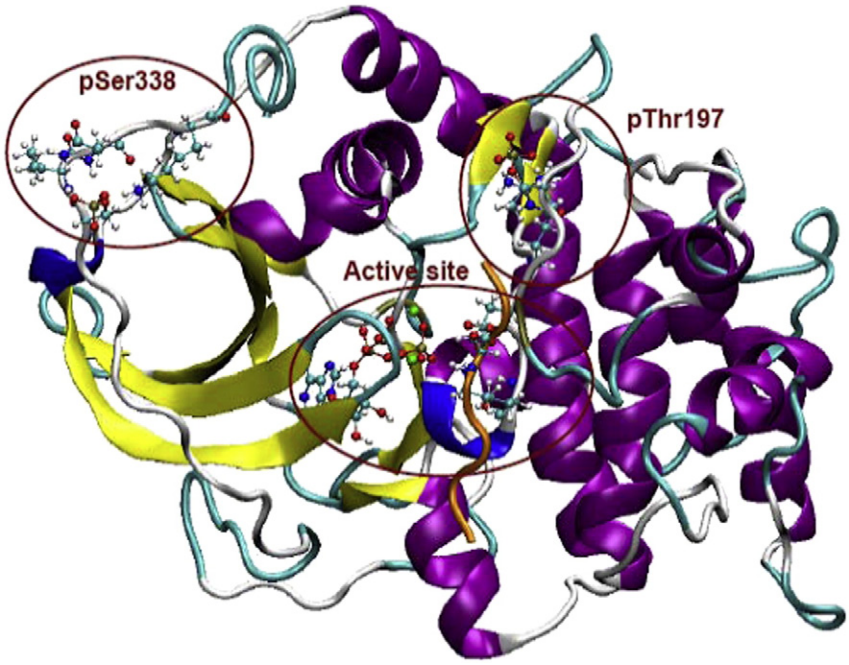

Fig. 6. Structure of 1ATP-Kemp Michaelis complex. The red circles highlight, from the top left, the position of pSer338, the position of pThr197, and the position of the active center.

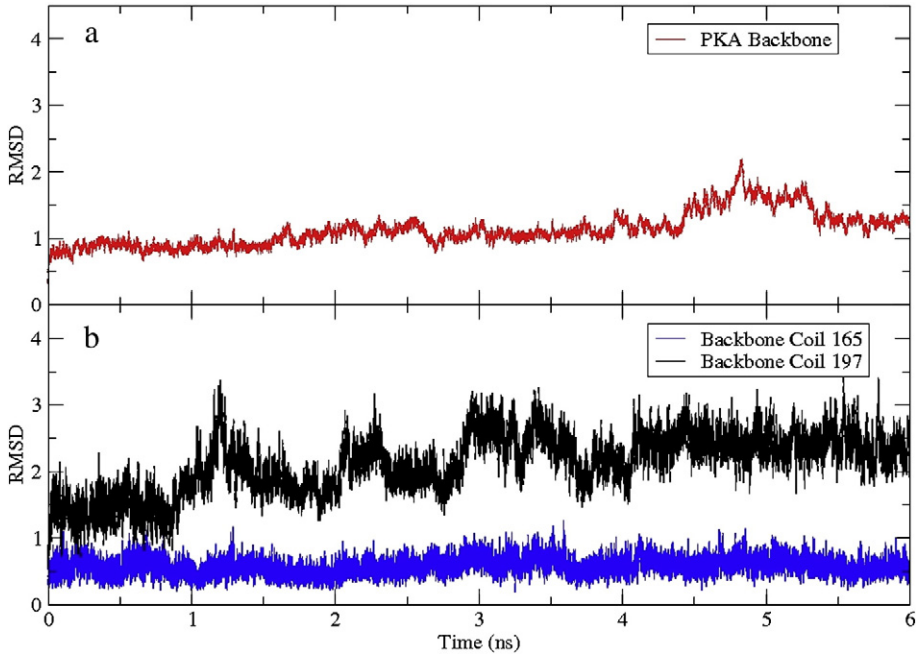

Fig. 7. RMSDs of a. PKA backbone and b. its two sub-selections in the 1CDK deactivated form of the enzyme.

configuration of Kemptide in the active center: the distance between P-ATP and O-Ser17kemp changes from 4.76 Å to 7.58 Å along the simulation (see Fig. 8) and the same trend is followed by all the other interaction distances of Kemptide analyzed in the previous subsections, as can be observed in Table S3. From the values in the Table it can be inferred that all the interactions required to hold the P-site of the substrate and to keep it in the active center become significantly weak when Lys168 and Asp166 get closer to each other as if they were acting as a gate to the catalytic site of the enzyme. All these results suggest why the unphosphorylated enzyme is not active.

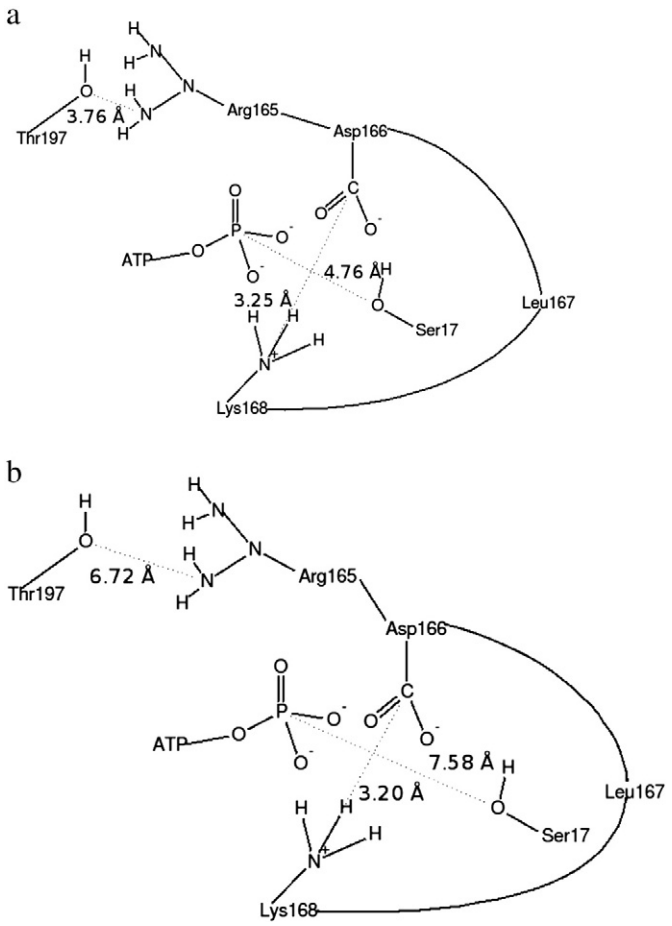

Fig. 8. Main interaction distances schemes of the 1CDK deactivated model: a. beginning of the MD simulation; b. end of the MD simulation.

3.4. 1CDK mutant D166A

Following the guideline of the preceding subsection we have studied another modified model of the holoenzyme. In this case the Asp166 residue has been mutated to an alanine residue, hence the name D166A for this model.

In Fig. 10 the RMSDs of the backbone of the enzyme and of the two regions of it named coil 165 and coil 197 are depicted. Observing the trend of the whole backbone (red line), once again we have found a slow but stable rise of the RMSD value along the entire simulation, similar to the 1CDK deactivated model. The difference is that this unnatural modification (it must be underlined that the previous modification was just a deactivation and not a mutation) leads to greater rearrangement of the global structure: indeed, the final RMSD value reached after 11 ns is slightly higher than 2 Å, which is the expected behavior for a deactivated form. Nevertheless, the local effect of the mutation on the coils 197 and 165 is somewhat different than in the deactivated form. First of all, it can be seen that the effect on the coil 197 (black line) is not as exaggerated as in the preceding model: the magnitude of the RMSD reaches a value of about 2 Å at the end of the simulation, and the rise is probably due to a little rearrangement in the configuration, as the two distances between the guanidinium nitrogen atoms of Arg165 and the oxygen atoms of pThr197 are maintained at about 2.7 Å along the whole simulation. Indeed, the effect of the mutation on the coil 165 is probably the most interesting at this point: the substitution of Asp166 leads to the destabilization in the area of the catalytic center, but the overall effect seems to be more subtle than it could be expected. In fact the rise of the value is quite small along the 11 ns. It goes from the initial value of about 0.5 Å to the final RMSD of approximately 1 Å. The only noticeable movement in the backbone is due to the loss of the interactions between the residue 166 and the other residues in the

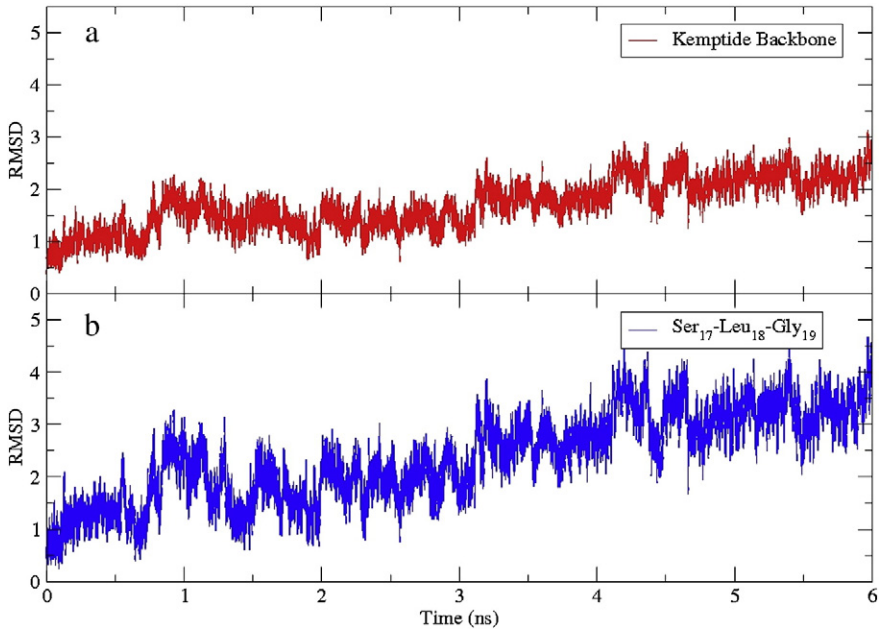

Fig. 9. RMSDs of a. Kemptide backbone and b. the backbone of the 3-residue C-terminus of Kemptide for 1CDK deactivated form of the enzyme.

catalytic center, and the consequent relaxation of the coil 197 connected to the coil 165 through Arg165.

As done before, we now focus on the RMSD of the Kemptide depicted in Fig. 11. It is not surprising to notice a rise of the RMSD. Interestingly, the major change of the whole peptide, and most importantly, of the C-terminal section (blue line), takes place at about 3 ns, just at the same time that the RMSD of coil 165 starts rising. Keeping this fact in mind, we can now analyze the distances between the alcoholic oxygen of the P-site residue and the other non-mutated residues.

The distances between $O_{\gamma\text{-Ser17-kemp}}$ and the other residues in the active center are represented in Fig. 12. Comparing the data in Fig. 12 with their counterpart in the previous subsection (Fig. 8), it is clear that the effect of the aspartate to alanine mutation leads to the opposite effect than the one occurred when deactivating the enzyme. In fact, it can be observed that the interaction between the Ser17 and the ATP molecule becomes stronger and the other interactions become slightly weaker, but still present, with the general disposition of the catalytic center resembling the associative mechanism

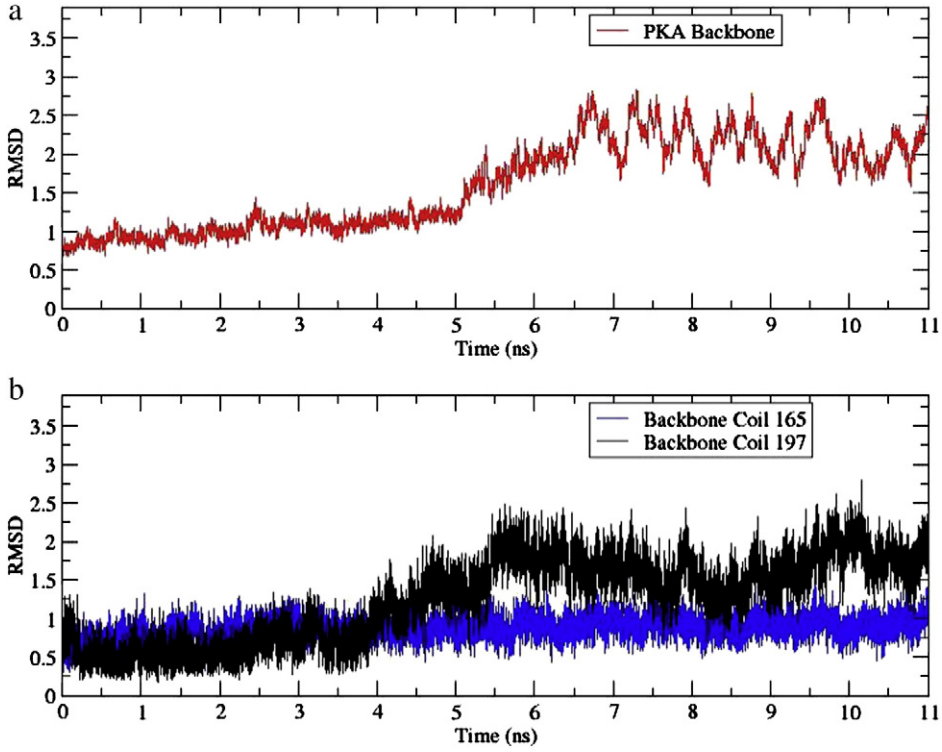

Fig. 10. RMSDs of a. PKA backbone of the 1CDK D166A mutant and b. its two sub-selections.

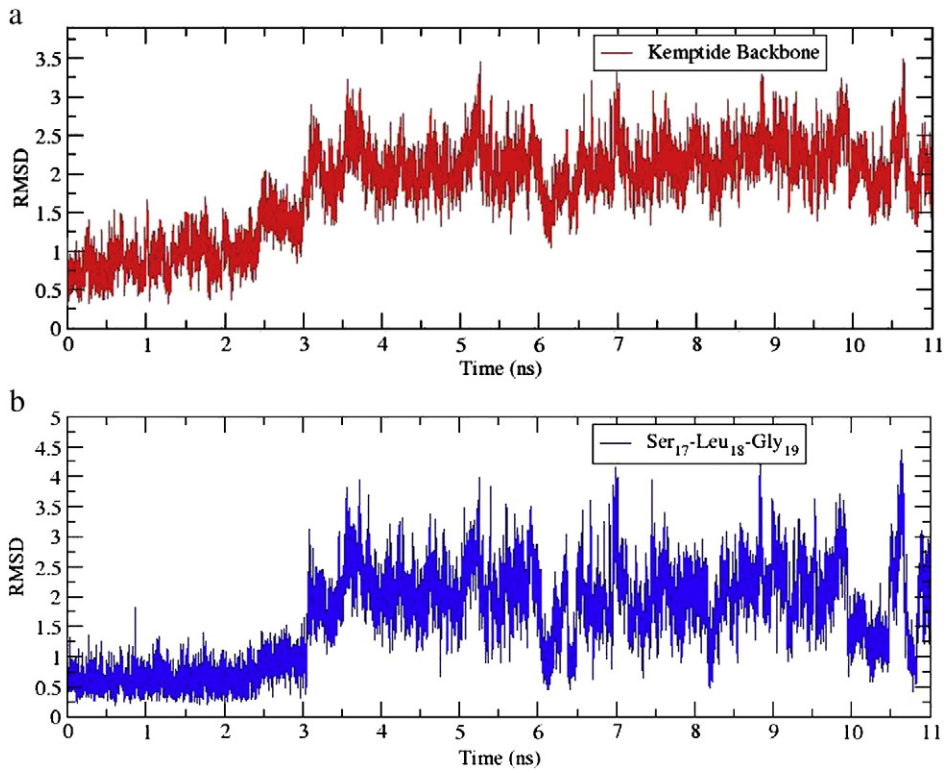

Fig. 11. RMSDs of a. Kemptide backbone and b. the backbone of the 3-residue C-terminus of Kemptide for the 1CDK D166A mutant form of the enzyme.

prereactive state. Indeed, we know from experimental works, that the mutation of Asp166 to Ala166 noticeably lowers the k_{cat} of the reaction [5]. From our results, we conclude that this is, in part, due to the weakened interaction of the negative moieties acting in the reaction with the positive and flexible side chain of Lys168, needed to coordinate the movement of the γ-phosphoryl group along the transfer from the ATP molecule to $Ser17_{Kemp}$; and, in part, due to the unfeasibility of the dissociative reactive channel. On the other hand, a role of $Asp166_{PKA}$ in the associative mechanism at a certain level can also be derived from these results: it may in fact, not only stabilize the side chain of Lys168PKA in its position, but also facilitate with its negative charge the abstraction of the moving proton.

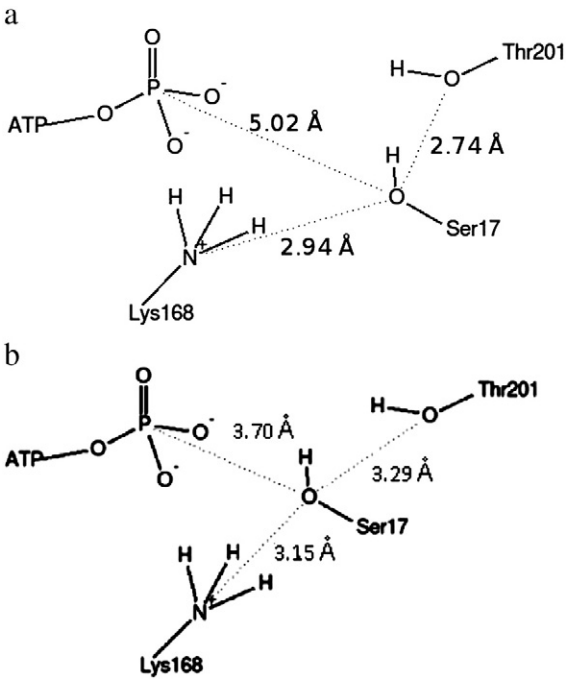

Fig. 12. Main interaction distances schemes of the 1CDK D166A mutant model: a. beginning of the MD simulation; b. end of the MD simulation.

4. Conclusions

In this work, we have identified the overall effect of the phosphorylation state of the enzyme: under the light of the results obtained, the first phosphorylation site of the PKA, Thr197, seems to be absolutely necessary for the functioning of the entire system. We have in fact observed that all the models with a phospho-threonine instead of a threonine in the 197th position can reach and maintain an active configuration of the catalytic center. While, on the other side, the only model without such phospho-threonine, not only cannot keep the initial active configuration, but also experiences destabilization of the configuration of the substrate that then tends to escape from the active region. We have also noticed how the different phosphorylation states can influence the flexibility of the structure and thus the possibility to explore different conformational states. The singly phosphorylated model (1CDK) shows a good flexibility that permits the system to jump from a dissociative-like prereactive conformation to an associative-like one, while the doubly phosphorylated model is a little more rigid. It can still easily rearrange from the user built configuration to a prereactive configuration, but only one conformational state is reached and maintained all through the simulation.

Finally, we have observed the effect of the presence and the absence of the highly conserved residue Asp166. This residue seems to be crucial for the correct placement of the P-site of the substrate, through the interaction with $Lys168_{PKA}$. Also, it appears to have an active role in the regulation of the activity of the enzyme, by limiting the accessibility to the active center and especially to the γ-phosphoryl group of the ATP molecule. In the end, the conservation of Asp166 seems to affect the choice of the prereactive state: we must remind here that experimentally, the mutation of the Asp166 to Ala166

does not lead to the deactivation of the enzyme but to a decrease of the reaction rate through the reduction of the k_{cat} [5,9].

In fact, this work has been followed by a QM/MM reactivity study, based on the two models that show the needed stability to maintain a prereactive configuration and the necessary flexibility to explore the accessible configurational space, that are the 1CDK and the 1ATP-Kemp models. From 1CDK, that presents two moderately stable configurations along the equilibration, we have selected two initial structures for the reactivity study: one for the associative mechanism and one for the dissociative one. Instead, for 1ATP-Kemp, which maintains only one stable configuration along the MD simulation, we have selected one initial geometry to explore both reaction mechanisms.

In that study we have demonstrated that the two mechanisms are possible [24]. However, the associative mechanism is only viable for the 1CDK model, and its potential energy barrier height (23 kcal/mol) is comparable with that of dissociative mechanism for 1CDK. Instead, the value of the potential energy barrier for the associative mechanism in the doubly phosphorylated model is more than 4 times higher than that in 1CDK.

The difference between the two models is most likely due to the different degree of rigidity of 1CDK and 1ATP-Kemp, which has been demonstrated in the present study. The higher flexibility of 1CDK may in fact allow the reactants to move rather freely in the active center, thus permitting them to rearrange comfortably along the reaction path.

Acknowledgment

We are thankful for the financial support from the Spanish “Ministerio de Ciencia e Innovación” through project CTQ2008-02403/BQU, the “Ramon y Cajal” program (L.M.), and the “Generalitat de Catalunya” project 2009SGR409.

Appendix A. Supplementary data

Supplementary data to this article can be found online at doi:10.1016/j.bpc.2011.11.001.

References

[1] E.H. Fisher, E.G. Krebs, J. Biol. Chem. 216 (1955) 121.
[2] D.A. Johnson, P. Akamine, E. Radzio-Andzelm, Madhusudan, S.S. Taylor, Chem. Rev. 101 (2001) 2243.
[3] D.A. Walsh, J.P. Perkins, E.G. Krebs, J. Biol. Chem. 243 (1968) 3768.
[4] S.M. Van Patten, D.C. Ng, J.P.H. Th'ng, K.L. Angelos, A.J. Smith, D.A. Walsh, Proc. Natl. Acad. Sci. USA 88 (1991) 5383.
[5] C.S. Gibbs, M.J. Zoller, J. Biol. Chem. 266 (1991) 8923.
[6] B.D. Grant, J.A. Adams, Biochemistry 35 (1996) 2022.
[7] Y. Cheng, Y. Zhang, J.A. McCammon, Protein Sci. 15 (2006) 672.
[8] A.S. Mildvan, Proteins 29 (1997) 401.
[9] Madhusudan, E.A. Trafny, N.H. Xuong, J.A. Adams, L.F. Teneyck, S.S. Taylor, J.M. Sowadski, Protein Sci. 3 (1994) 176.
[10] L.R. Masterson, C. Cheng, T. Yu, M. Tonelli, A. Kornev, S.S. Taylor, G. Veglia, Nat. Chem. Biol. 6 (2010) 821.
[11] N. Diaz, M.J. Field, J. Am. Chem. Soc. 126 (2004) 529.
[12] L. R. Masterson, L. Shi, E. Metcalfe, J. Gao, S. S. Taylor, G. Venglia Proc. Natl. Acad. Sci. USA 108 (2011) 6969.
[13] M. Montenegro, M. Garcia-Viloca, À. González-Lafont, J.M. Lluch, J. Comput. Aided Mol. Des. 21 (2007) 603.
[14] B.E. Kemp, D.J. Graves, E. Benjamini, E.G. Krebs, J. Biol. Chem. 252 (1977) 4888.
[15] R. Qamar, M.-Y. Yoon, P.F. Cook, Biochemistry 31 (1992) 9986.
[16] J.A. Adams, M.J. Moore, S.S. Taylor, J. Biol. Chem. 278 (2003) 10613.
[17] D. Bossemeyer, R.A. Engh, V. Kinzel, H. Ponstingl, R. Huber, EMBO J. 12 (1993) 849.
[18] J. Zheng, D.R. Knighton, L.F. Ten Eyck, R. Karlsson, N.-h. Xuong, S.S. Taylor, J.M. Sowadski, Biochemistry 32 (1993) 2154.
[19] Y. Cheng, Y. Zhang, J.A. McCammon, J. Am. Chem. Soc. 127 (2005) 1553.
[20] H. Li, A.D. Robertson, J.H. Jensen, Proteins 61 (2005) 704.
[21] A.D. Jr, D. MacKerell, M. Bashford, R.L. Bellott, J.D. Dumbrack Jr., M.J. Evanseck, S. Field, J. Fischer, H. Gao, S. Guo, D. Ha, L. Joseph-MacCarthy, K. Kuchnir, F.T.K. Kuczera, C. Lau, S. Mattos, T. Michnick, D.T. Ngo, B. Nguyen, W.E. Prodhom, B. Reiher III, M. Roux, J.C. Schlenkrich, R. Smith, J. Stote, M. Straub, J. Watanabe, D. Yin Wiórkiewicz-Kuczera, M. Karplus, J. Phys. Chem. B 102 (1998) 3586.
[22] B. Brooks, R. Bruccoleri, B. Olafson, D. States, S. Swaminathan, M. Karplus, J. Comput. Chem. 4 (1983) 187;
B.R. Brooks, C.L. Brooks, A.D. Mackerell, L. Nilsson, R.J. Petrella, B. Roux, Y. Won, G. Archontis, C. Bartels, S. Boresch, A. Caflisch, L. Caves, Q. Cui, A.R. Dinner, M. Feig, S. Fischer, J. Gao, M. Hodoscek, W. Im, K. Kuczera, T. Lazaridis, J. Ma, V. Ovchinnikov, E. Paci, R.W. Pastor, C.B. Post, J.Z. Pu, M. Schaefer, B. Tidor, R.M. Venable, H.L. Woodcock, X. Wu, W. Yang, D.M. York, M. Karplus, J. Comput. Chem. 30 (2009) 1545 M. H. Feng, M.
[23] Philippopoulos, A.D. MacKerell, C. Lim, J. Am. Chem. Soc. 118 (1996) 11265.
[24] M. Montenegro, M. Garcia-Viloca, J.M. Lluch, A. González-Lafont, Phys. Chem. Chem. Phys. 13 (2011) 530.